Applied Catalysis B: Environmental 142–143 (2013) 662–667

Contents lists available at SciVerse ScienceDirect

Applied Catalysis B: Environmental

journal homepage: www.elsevier.com/locate/apcatb

TiO_2 suspension exposed to H_2O_2 in ambient light or darkness: Degradation of methylene blue and EPR evidence for radical oxygen species

Luis Domínguez Sánchez[a], Sébastien Francis Michel Taxt-Lamolle[a], Eli Olaug Hole[b], André Krivokapić[b], Einar Sagstuen[b], Håvard Jostein Haugen[a,*]

[a] Department of Biomaterials, Institute for Clinical Dentistry, University of Oslo, PO Box 1109, Blindern, Oslo N-0317, Norway
[b] Department of Physics, University of Oslo, PO Box 1048, Blindern, Oslo N-0316, Norway

ARTICLE INFO

Article history:
Received 23 November 2012
Received in revised form 25 April 2013
Accepted 9 May 2013
Available online 23 May 2013

Keywords:
TiO_2
H_2O_2
Catalysis
Reactive oxygen species
EPR spin trapping

ABSTRACT

The photocatalytic behaviour of TiO_2 has been thoroughly investigated the past years using UV light to photoactivate TiO_2. As this method introduces complications making it difficult to do it economically viable, new pathways to activate TiO_2 have been sought. In the present work, reactive oxygen species (ROS) were obtained in a suspension of hydrogen peroxide (H_2O_2) and titanium dioxide (TiO_2) in darkness, offering an alternative method to initiate oxidative behaviour of TiO_2. Methylene blue (MB) degradation was chosen as an indicator for measuring the catalytic effect, allowing for a comparison of the reaction kinetics with other methods to create ROS with TiO_2. The effects of TiO_2 particle effective surface area and concentration of H_2O_2 were also studied. EPR studies were made to determine the presence of free radicals in the mixture of TiO_2/H_2O_2 in darkness. Under the given lighting conditions, the results demonstrate the relevance of the TiO_2 effective surface area and concentration of H_2O_2 and TiO_2 as parameters influencing the chemical catalysis of MB due to the action of hydroxyl ($OH^\bullet$) and/or hydroperoxide radicals ($HO_2^\bullet$).

1. Introduction

During the last years, heterogeneous photocatalysis based on TiO_2 particles and UV-light has been investigated as a method for removing hazardous chemical substances in water [1] and for disinfection [2]. Several kinetic studies have been conducted to elucidate the reaction mechanisms [3–6]. All these suggested that $OH^\bullet$ radicals were produced through the interaction between water (H_2O) and photoactivated TiO_2, the reaction efficiency being controlled by the number of photoactivated TiO_2 sites. Recently, a new way to activate the TiO_2 particles based on ultrasound stimulation was reported. Wang and co-workers analysed the formation of reactive oxygen species (ROS) by TiO_2 particles under ultrasonic irradiation and the action of these radicals on organic dyes, including methylene blue (MB) [7]. Apparently, these organic dyes are degraded via first order kinetics [7], and photoactivated TiO_2 degrades MB with the same reaction kinetics [8].

The oxidative reaction is improved by adding H_2O_2 in sono and photocatalysis, respectively [9,10]. Rincón and co-workers found how TiO_2 could increase the bactericide action of H_2O_2 on *Escherichia coli* in darkness [11]. MB was exposed to a mixture of TiO_2 and H_2O_2, in darkness [12] and with ambient light [13]. Furthermore, Ogino et al. suggested the production of titanium peroxide through the interaction of TiO_2 and H_2O_2 and demonstrated the oxidative effect on MB without light [14]. On the other hand, there are studies demonstrating the opposite effect [15–17]. Due to this ambiguity, it was considered necessary to explore further the interactions between H_2O_2 and TiO_2. MB has proven useful for investigating the photocatalytic activation of TiO_2 due to its high visible light absorbance allowing an easy detection of chemical changes to the dye, even at low concentrations.

The aim of the present work was to investigate the kinetic degradation of MB exposed to a mixture of TiO_2 and H_2O_2. Particular emphasis was put on the importance of the effective surface area of the TiO_2 particles and the influence of the absence of light in the process. EPR spin trapping techniques were used to elucidate the formation of ROS in the process.

2. Experimental

2.1. Materials

Micro and nano-sized TiO_2 particles were used in the present work. The nano-sized TiO_2 (Degussa Aeroxide P25,

* Corresponding author. Tel.: +47 22852350; fax: +47 22852351.
E-mail addresses: h.j.haugen@odont.uio.no, haavardhaugen@online.no (H.J. Haugen).

0926-3373/$ – see front matter © 2013 Elsevier B.V. All rights reserved.
http://dx.doi.org/10.1016/j.apcatb.2013.05.017

Hanau-Wolfgang, Germany) BET area (BET theory aims to explain the physical adsorption of gas molecules on a solid surface) was previously measured in 50 m^2/g. The particles exhibit a D_{50} of 21 nm, and a crystalline structure of anatase (80%) and rutile (20%) [18]. The micro-sized TiO_2 (Kronos 1171, Kronos Titan AS, Fredriksten, Norway) BET area was measured to be 8.82 m^2/g per particle [19]. These particles exhibit anatase (99%) crystalline structure, and particles with D_{50} of 100–180 μm were used.

MB laboratory reagent and H_2O_2 (9.8 M) were obtained from Sigma–Aldrich (Steinhem, Germany). Solutions and suspensions were prepared using deionised water (Millipore, Billerica, MA, USA). To remove distortions related to changes in fluid mechanics, the procedure aimed at reproducibility of flow (laminar or turbulent).

2.2. Methylene blue degradation

For the measurements in ambient light, a magnetic stirrer was introduced in the beaker (⌀ = 6.5 cm) before it was filled with the right amount of 9.8 M H_2O_2 (4 °C) and deionised water (room temperature) in each case for a total volume of 20 mL. At this point, from 0.08 to 1.28 g of TiO_2 (nano or micro)-powder was added and the mixture was stirred for 2 min at 1100 rpm. Then, 20 mL of 0.3 mM MB was added and the suspension was stirred for another minute. An aliquot of 1 mL was then immediately taken from the mixture, introduced in an Eppendorf tube and centrifuged (Labnet International Inc., C1301-230V, Edison, NJ, USA) for 1 min. The supernatant was extracted and introduced in a 1.5 mL cuvette to be analysed in a UV-Vis spectrophotometer (Lambda 25, Perkin Elmer instruments, Waltham, MA, USA). After the analysis, the liquid in the cuvette and the powders in the Eppendorf tube were returned to the beaker. The procedure starting with the 1 mL aliquot extraction was repeated (at least) every 10 min for maximum 1 h. The entire procedure was repeated three times for every particle size and TiO_2, H_2O_2 concentration.

An initial study was conducted to clarify which of the 609 nm and 668 nm absorption peaks of MB, and also which order of kinetics, were the most appropriate. This was judged from the coefficient-of-determination (r^2) obtained by fitting the UV-VIS data for the degradation of the dye using Eqs. (1) and (2) below. The data analysis showed a slightly better r^2 using second order kinetics (Eq. (2)) for the 609 nm peak degradation of MB as compared to using first order kinetics (Eq. (1)) for the 668 nm MB peak degradation.

$$B_t = B_0 \cdot e^{-k \cdot t} \quad (1)$$

$$\frac{1}{B_t} - \frac{1}{B_0} = k * t \quad (2)$$

For the experiments in darkness, 2 beakers (⌀ = 6.5 and 10 cm) were placed concentrically into each other. To immobilize the inner beaker, black polyurethane foam was placed between the walls of the two vessels. Also, a cover of the same material with ⌀ = 10 cm and thickness 1.5 cm was placed on the top of the beakers. In the cover, a hole (⌀ = 0.5 cm) close to the inside wall of the inner container facilitated sample collection in the vortex formed during the agitation of the mixture. This entrance was also used for adding components of the mixture with the aid of a funnel. Finally the larger vessel was covered with aluminium foil to prevent any light exposure to the mixture. A different procedure was used to obtain samples for later analysis in the spectrophotometer. These changes only concern the procedure of mixing the reagents, aiming at reducing the possible influence from any exposure of light to the samples analysed [20]. The inner beaker was filled with 20 mL 0.3 mM MB and 0.16 g of TiO_2 and stirred for 10 min before adding 20 mL 9.8 M H_2O_2. After stirring for another minute, sampling started following the original procedure. The ambient light was kept as low as possible during these procedures.

2.3. EPR experiments

For the EPR experiments some modifications were made to the darkness-experimental procedure above. The mixtures of TiO_2 (10 g/L) and H_2O_2 (9.8 M) were stirred at 1100 rpm for 5 min in complete darkness using the methodology applied in the dark experiments. Under the lowest possible ambient lighting, a 2 mL sample was taken with a Pasteur pipette and introduced into an Eppendorf tube. The tube was centrifuged for 1 min and using a Pasteur pipette the supernatant was removed. 0.5 mL of 0.2 M DMPO (Sigma–Aldrich, Steinhem, Germany) was immediately added to the precipitate and the tube was shaken by hand to ensure homogenization of the sample. Then, about 0.05 mL of this sample was introduced in a 1.7 mm OD capillary for immediate EPR analysis in complete darkness.

The EPR measurements were made using a BRUKER (Rheinstetten, Germany) EleXsyS 560 X-band spectrometer equipped with a standard rectangular TE_{102} cavity. A 4 mm outer diameter 707-SQ-250 quartz tube (WILMAD, Vineland, NJ, USA) was used to support the capillary tubes and Teflon pedestals were used to support the 4 mm tube to reproducible positions in the cavity. For the measurements, an 8 mT field scan was used with a field modulation frequency of 100 kHz and modulation width of 0.1 mT. The microwave frequency typically was about 9771 MHz and the centre field was 348.5 mT. The field scan rate was 0.19 mT/s and the time constant was 0.16 s. The microwave power was 12.6 mW. 2 scans were added for each complete spectrum acquisition unless otherwise indicated.

2.4. Statistics

Normality (Shapiro–Wilko) and equal variance tests were performed on the dataset from the MB degradation. All datasets failed normality and were thus analysed using non-parametric Kruskal–Wallis one-way ANOVA with multiple comparisons performed. Statistical significance was considered at a probability $p < 0.05$. All statistical analyses were performed using SigmaPlot 12 (Systat Software Inc., San Jose, USA). For datasets that failed the normality test, the median (Q2) and interquartile range (IQR), being equal to the difference between the upper and lower quartiles Q3–Q1, were presented.

3. Results and discussion

3.1. Reaction kinetics, ambient lightning

Nearly no degradation of MB was observed when exposed to 1.6 M H_2O_2 alone (see Fig. 1). Almost the same result was obtained with 4.9 M H_2O_2. The slight decrease in the 609 nm absorbance was not reflected in the 668 nm peak, which remained stable. This suggests not only a slight degradation of the sample, but can also indicate that the MB dimer is degraded before the MB monomer. That may also explain why the second order fitting of the 609 nm peak degradation exhibits a slightly better r^2 than the first order fitting of the 668 nm peak degradation. Some studies suggest that the adsorption of MB on the surface of TiO_2 (anatase) occurs when the dye is in its dimeric form [21,22]. Since adsorption usually is the factor controlling the kinetics in heterogeneous catalysis, these studies support the aggregation of MB on the TiO_2 surface. However, the interference on the spectrum signal of TiO_2 particles and/or intermediates during degradation of MB [23] prevents a firmer conclusion.

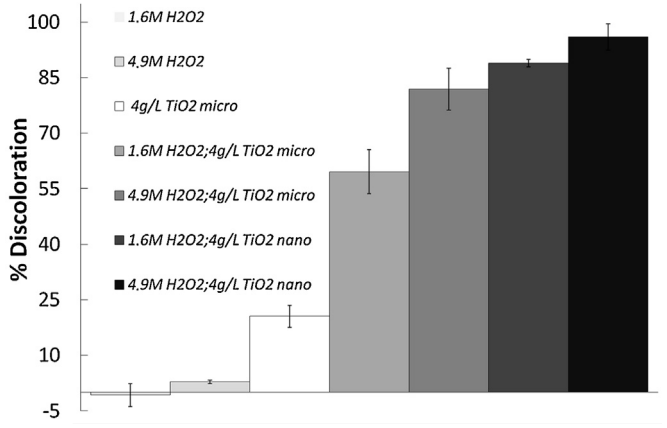

Fig. 1. The decolouration process of MB in 1 h with ambient light using 4 g/L of nano or micro TiO_2 particles interacting with 4.9 or 1.6 M H_2O_2 solutions, showing mean values of three samples. Blank tests were also done with 4.9 or 1.6 M H_2O_2 solutions alone and 4 g/L of micro TiO_2 particles alone. The fully drawn curves are the result of fitting Eq. (2) (see text). All analyses were made at 609 nm.

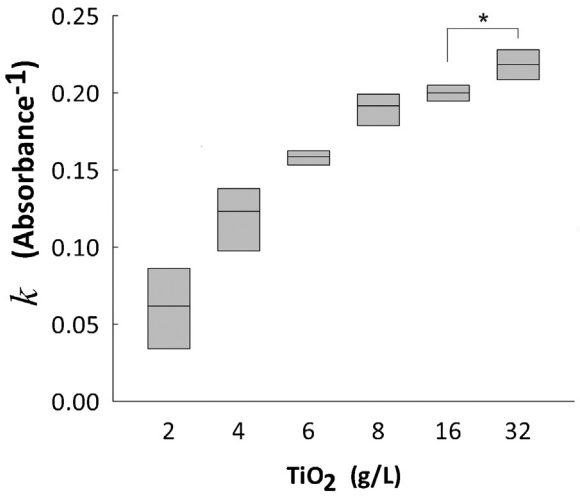

Fig. 2. Degradation of MB (609 nm) when exposed to a mixture of 1.6 M H_2O_2 and increasing concentrations of TiO_2 nano particles under ambient light. All groups were found to be statistically significant against each other except for group labelled * ($n = 3$).

It should be noted that in nano-sized TiO_2 suspensions, the results with respect to the kinetic order of the degradation of MB were inconclusive since the sedimentation by centrifugation was impossible due to flocculation (further discussed in Section 3.2). However Zhang and co-workers reported no degradation of MB with TiO_2 only, using an alternative method to separate the particles from the liquid [8]. The same observation was made using the micro particles. However, the particle size facilitated their precipitation, allowing interpretable results. In this case, the small degradation observed can be interpreted as an effect of the photocatalyst and/or adsorption of the dye on the TiO_2's surface.

The results in Fig. 1 demonstrate synergetic oxidative effects of H_2O_2 and TiO_2 and suggest a chemical interaction between TiO_2 and H_2O_2. Using the data in Fig. 1, the second order kinetics of the MB degradation was probed at 609 nm by fitting Eq. (2). In all instances, Eq. (2) provided the best fit. The fitting results are shown in Table 1.

The second order kinetics observed is different from that obtained for the sono-activation [7] and photo-activation mechanisms [3,24]. However, the initial study performed (see paragraph above) to elucidate which is the best reaction order and absorption peak to use for obtaining the best coefficient of determination in the linear regression only showed a slight improvement between the second order fitting of the 609 nm peak degradation and the first order 668 nm peak degradation. Furthermore, the conclusions that can be made from the previous works are analogous to those obtained in the present article. It may therefore be possible to compare the present results using Eq. (2) on the 609 nm peak with those using other known methods to create ROS through TiO_2 analysed by using Eq. (1) on the 668 nm peak.

3.2. Influence of relative surface area and TiO_2/H_2O_2 ratio

High standard deviations in some of the data were observed. It was concluded that the most plausible explanation for this is related to agglomeration or flocculation due to the interaction between the TiO_2 and H_2O_2 as mentioned in other studies [25,26]. During the experiments, it was observed that TiO_2 particles tended to agglomerate at high H_2O_2 concentration (4.9 M *versus* 1.6 M) as the mixtures with low H_2O_2 contents were easier to precipitate during centrifugation. Moreover, at a given H_2O_2 concentration, increasing concentration of nano-sized TiO_2 particles enhanced the precipitation.

Nevertheless, it is clear that the TiO_2 effective surface area as well as TiO_2 and H_2O_2 concentrations influence the oxidative effect. This is evidenced by the observations that using nano-sized TiO_2 instead of micro-sized TiO_2 particles increased the degradation rate of MB at equal H_2O_2 concentrations (Fig. 1). The data presented in Fig. 2 demonstrate the same trend, showing that for constant H_2O_2 concentration the degradation of MB as a function of the TiO_2 concentration increased until a kind of saturation was observed. It may be speculated that this behaviour is due to an apparent saturation of the H_2O_2/TiO_2 interaction when the ratio between the TiO_2 and H_2O_2 concentrations increases beyond a certain range.

In order to confirm the validity of the results, the adsorbability of MB on TiO_2 was investigated. The constant concentration of MB allowed us to relate the relative surface concentration of TiO_2 with the crystal structure of the oxide. Of particular interest in this connection is the work of Kapinus et al. [27] which presents

Table 1
Linear regression values corresponding to a second order kinetics of the methylene blue's (MB) decolouration. The data are represented as the percentage of discolouration produced in 1 h in Fig. 1. The presented data are median (Q2) and interquartile ranges.

Particle size	H_2O_2 (M)	k (min abs^{-1})	B_0^{-1} (abs^{-1})	r^2 mean
Nano	1.6	0.06590 (0.06520;0.06795)[a]	0.237 (0.212;0.286)	0.989 (0.988;0.990)
	4.9	0.25330 (0.23565;0.26315)[a]	0.905 (0.834;0.985)[a]	0.981 (0.975;0.989)
Micro	1.6	0.01100 (0.01075;0.01270)[a]	0.503 (0.493;0.518)	0.988 (0.981;0.989)
	4.9	0.05330 (0.05255;0.05580)[a]	0.287 (0.263;0.323)	0.964 (0.955;0.980)
None	1.6	−0.00003 (−0.00008;0.00002)[a]	0.278 (0.274;0.282)	0.226 (0.196;0.458)
None	4.9	0.00014 (0.00013;0.00017)[a]	0.354 (0.353;0.359)	0.957 (0.950;0.968)
Micro	None	0.00129 (0.00118;0.00141)[a]	0.306 (0.303; 0.311)	0.974 (0.974;0.982)

[a] $p < 0.05$ when there is a statistical difference with the rest of the groups, k = slope of curve, B_0^{-1} = interception point. The fully drawn curves are the result of fitting Eq. (2) (see text). All analyses were made at 609 nm.

Table 2
Summary of the EPR results obtained.

Sample composition	TiO_2 type	Detected radicals[a]	Comments
DMPO[b] + H_2O_2 + TiO_2[c]	P25 (nano)	$HO_2^\bullet$ (+), $OH^\bullet$ (nd)	Fig. 4. $HO_2^\bullet$ decaying
	Kro (micro)	$HO_2^\bullet$ (w), $OH^\bullet$ (+)	Fig. 5. $OH^\bullet$ growing in
DMPO + TiO_2 + water	P25 (nano)	$OH^\bullet$ (w)	
	Kro (micro)	(nd)	
DMPO + H_2O_2	–	$OH^\bullet$ (w)	
DMPO + supernatant	–	$OH^\bullet$ (w)	
DMPO + H_2O_2 + 5*TiO_2[d]	Kro (micro)	$HO_2^\bullet$ (+), $OH^\bullet$ (nd)	Fig. 7. $HO_2^\bullet$ decaying
DMPO + H_2O_2 + (1/5)*TiO_2[e]	P25 (nano)	$HO_2^\bullet$ (w), $OH^\bullet$ (w)	Fig. 6. $OH^\bullet$ growing in

[a] (+) dominant signal; (w) weak signal; (nd) not detectible or very weak.
[b] 200 mM.
[c] In the initial mixture, 10 g/L.
[d] The amount of TiO_2 was increased with a factor of 5 relative to the initial mixture.
[e] The amount of TiO_2 was reduced with a factor of 5 relative to the initial mixture.

interesting results on the adsorption of MB on the TiO_2 surfaces (anatase and rutile). These authors found that when the particle size and specific surface is constant, the mixture of both crystal structures shows a behaviour similar to that of anatase alone, while the rutile structure alone has a 10 times smaller capacity to adsorb MB as compared to the anatase structure. Other papers are supporting the conclusions of Kapinus and co-workers [12,28]. For this reason, the crystal structure was discarded as a factor which can influence the dye adsorbability in the present work.

3.3. Measurements in darkness

When corresponding experiments were done in the dark, the efficiency in the degradation of MB was somewhat reduced as compared with the results obtained in ambient light. This is demonstrated in Fig. 3 which indicates only a slight improvement (around 20–25%) in the degradation of MB in the presence of ambient light. Even if light sensitive degradation of the dye by TiO_2 is well known [29], the improvement shown in Fig. 3 may not necessarily be attributed to the action of light alone as other factors, such as the adsorption on TiO_2, may depend on changes in the procedures necessary to eliminate light. Regardless, it is clear that light is not a necessary factor for the MB degradation process.

3.4. Presence of free radicals

The results obtained using the spin-trap EPR methods show the presence of free radicals in the absence of light. The radical species trapped were identified as hydroxyl ($OH^\bullet$) and superoxide ($O_2^{\bullet-}$) or hydroperoxyl ($HO_2^\bullet$) radicals. Table 2 summarizes the most salient features of the results obtained.

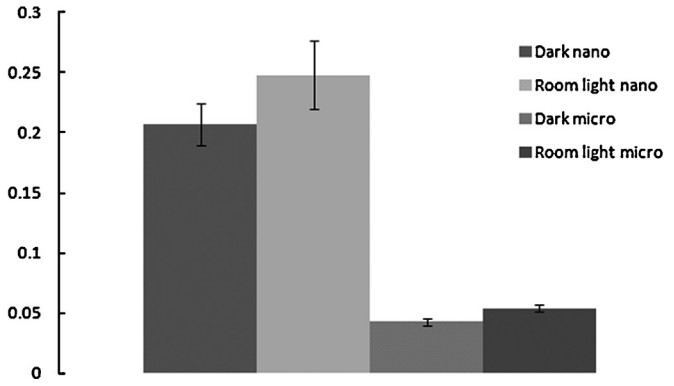

Fig. 3. Second order kinetic degradation slopes of MB (609 nm) using 4 g/L nano or micro TiO_2 particles interacting with 4.9 M H_2O_2 solution with ambient lighting or in complete darkness, showing mean values of three samples.

It is important to note that data presented here should only be considered qualitatively since the procedure used renders the exact concentration of H_2O_2 unknown. Furthermore, it is spectroscopically difficult to differentiate between the spin adducts of the superoxide ($O_2^{\bullet-}$) and the hydroperoxyl ($HO_2^\bullet$) radicals when using DMPO as a spin trap [30]. Brezova and co-workers reported that radical formation in the photoinitiated oxygen-saturated TiO_2 system is frequently monitored by various spin traps (DMPO, TMPO, POBN and MePyBN), but due to their consecutive reactions these bring less reliable information on the real photocatalytic activity of TiO_2 [31]. Nevertheless, the current method provided evidence of the free radicals hydroxyl ($OH^\bullet$) and superoxide ($O_2^{\bullet-}$) or hydroperoxyl ($HO_2^\bullet$) radicals.

The pK_a value for the hydroperoxl radical is 4.8 [32]. In the MB degradation experiments the pH was always below 4, being even lower when the TiO_2 concentration was increased. For this reason, it was concluded that the observed species is most probably the DMPO-trapped hydroperoxyl radical. It may be commented that the trapping rate constant for DMPO to the hydroxyl and superoxide/hydroperoxyl radical differs with 8 orders of magnitude at pH = 7 (3.4×10^9 and 60, respectively) [33]. This may shift the relative yields of the trapped ROS as measured from the corresponding EPR signals away from the stoichiometric composition in some instances. All experiments were made in darkness.

3.4.1. TiO_2 and H_2O_2 trapping experiments

Figs. 4 and 5 show the results obtained using P25 and Kronos TiO_2 particles, respectively. Whereas the P25 particles led to a signal due to trapped hydroperoxyl radicals alone, the Kronos particles yielded a signal mainly due to trapped hydroxyl radicals. The coupling constants for the two radicals are close to those published in the literature, for the hydroperoxyl ($HO_2^\bullet$) radical the present spectra yielded A_N = 1.42 mT, aH^β = 1.12 mT and aH^γ = 0.12 mT. For the hydroxyl ($OH^\bullet$) radical, $a_N = aH^\beta$ = 1.48 mT.

It may be suspected that the difference in response for the P25 and Kronos particles may be due to the 5-fold increased effective area of the P25 as compared to that of the Kronos particles. Therefore, two new experiments were designed. First, the amount of P25 TiO_2 particles was reduced with a factor of 5 with respect to the initial amount (10 g/mL). Second, the amount of Kronos TiO_2 particles was increased with a factor of 5 with respect to the initial amount. For these two cases, the effective areas are now comparable. The results are shown in Figs. 6 and 7, respectively. It is interesting that the Kronos experiment (Fig. 7) now yields a virtually pure hydroperoxyl ($HO_2^\bullet$) radical signal indicating that the effective area available for exposure to H_2O_2 is crucial for the nature

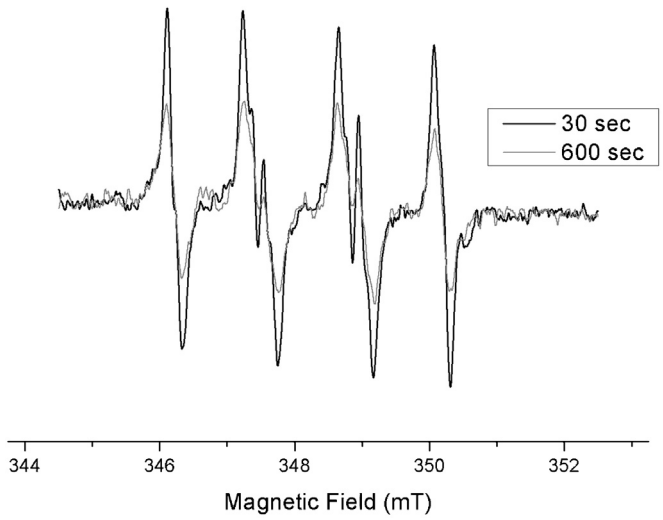

Fig. 4. X-band EPR spectra from H_2O_2 suspensions of P25 TiO_2 nanoparticles with DMPO spin trap. The signal is an almost clean signal characteristic for hydroperoxyl radical ($O_2H^\bullet$) trapping by DMPO. The two spectra were recorded at the indicated times after the samples were transferred to the EPR cavity.

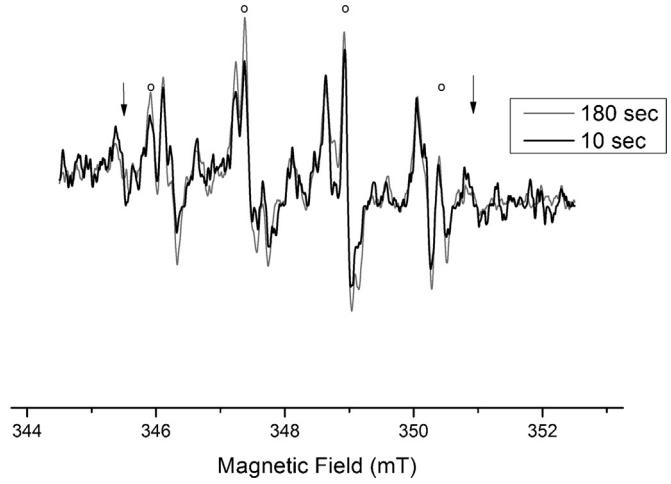

Fig. 6. X-band EPR spectra from H_2O_2 suspensions of P25 TiO_2 nanoparticles with DMPO spin trap. The amount of TiO_2 is reduced with a factor of 5 as compared to Fig. 4. The EPR signal due to the trapped hydroxyl ($OH^\bullet$) radicals are marked by small circles. This signal overlaps with the signal due to trapped hydroperoxyl ($O_2H^\bullet$) radicals. Outer wing lines (marked with arrows) belong to a more complex spectrum due to oxidized DMPO (see also Fig. 5). The two spectra were recorded at the indicated times after the samples were transferred to the EPR cavity.

of the ROS produced. The P25 experiment (Fig. 6) was not similarly ubiquitous, here some hydroperoxyl radicals are still present, but now a comparable amount of hydroxyl ($OH^\bullet$) radicals are observed (lines in spectra marked by small circles). It should be noted that in Figs. 5 and 6 some additional weak lines are observed on the wings of the spectra (marked by arrows in Fig. 6) that probably are due to oxidized DMPO [34]. The two wing lines indicated are accompanied by 4 other lines in the middle of the spectrum.

It appears as if the ratio between the effective area of the TiO_2 particles and the volume of liquid controls the prevalence of the radical formed. High values of this ratio promote hydroperoxyl ($HO_2^\bullet$) radicals, low values favour hydroxyl ($OH^\bullet$) radicals. This fits with the discussion in the work of Lousada et al. [35] and was explained by the change in extent of decomposition of H_2O_2 on TiO_2. For high values of the ratio (where the presence of hydroperoxyl radicals prevails), very weak traces of hydroxyl radicals were observed. These $OH^\bullet$ radicals may be due to decomposition of the $HO_2^\bullet$ (hydroperoxyl) spin adduct. The differences found when comparing low effective area/volume ratios may be caused by multiple factors such as the presence of rutile in P25 or divergence of impurities and/or defects due to the manufacturing method of P25 and Kronos. However, referring to the finding by Du et al. [26], it is possible to speculate whether a loss of effective surface area due to an agglomeration of particles takes place. This would result in a reduced production of hydroxyl radicals. On the another hand, agglomeration is due to interactions between hydroperoxyl radicals ($HO_2^\bullet$) to the surface of TiO_2. For this reason, the presence of $HO_2^\bullet$ is stabilized at high concentrations of TiO_2. This model fits well with the results found with the EPR experiments and data presented in Fig. 2.

3.4.2. Blank test analysis

Tests on the formation of ROS demonstrated that it is possible to produce weak traces of hydroxyl ($OH^\bullet$) radicals also in the absence

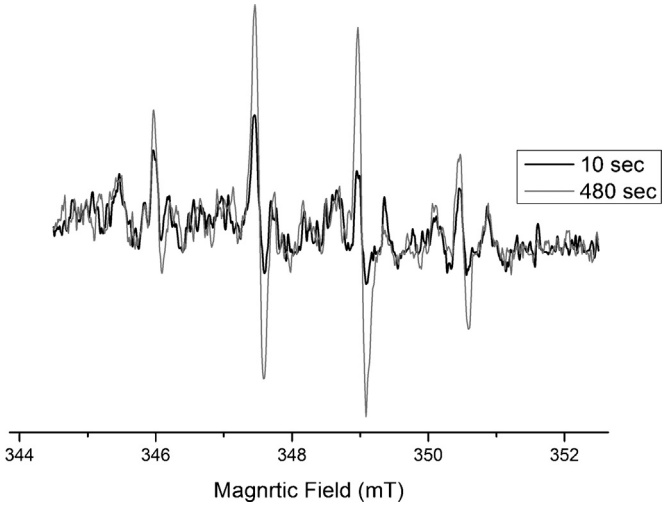

Fig. 5. X-band EPR spectra from H_2O_2 suspensions of Kronos TiO_2 microparticles with DMPO spin trap. The main signal is due to hydroxyl radical ($OH^\bullet$) trapping. The two spectra were recorded at the indicated times after the samples were transferred to the EPR cavity.

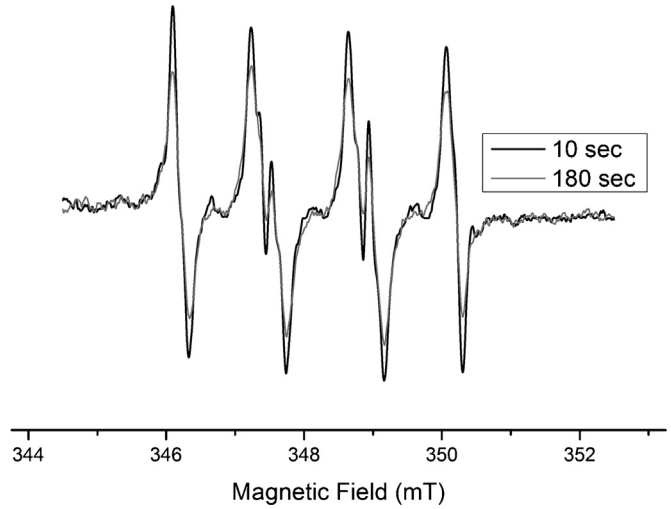

Fig. 7. X-band EPR spectra from H_2O_2 suspensions of Kronos TiO_2 microparticles with DMPO spin trap, showing a clean signal due to trapped hydroperoxyl ($O_2H^\bullet$) radicals. The amount of TiO_2 is increased with a factor of 5 as compared to Fig. 5. The two spectra were recorded at the indicated times after the samples were transferred to the EPR cavity.

of TiO_2. However, the absence of a corresponding catalytic effect in the MB degradation experiments suggests that the $OH^•$ radicals are produced by the interaction between H_2O_2 and DMPO, an effect which also has been observed previously [34]. In the absence of H_2O_2 but in the presence of TiO_2 the results are divergent. Kronos powders show no sign of trapped ROS, while P25 powders indicate weak traces of trapped hydroxyl ($OH^•$) radicals. This difference may be due to the BET area of P25 being 5 times greater than that of Kronos. Similar observations have been made previously [36]. Regardless, the minor amount of reactive oxidants produced without H_2O_2 or TiO_2 present apparently is insufficient to induce observable degradation of MB.

3.4.3. Presence of free radicals in the absence of light

In the present work it is demonstrated that ROS may be produced in the reaction of TiO_2 and H_2O_2 without the presence of light. These results do not support some of the results presented by Fenoglio et al. [37], as these authors relate the appearance of free radicals in the absence of light to the rutile structure of TiO_2. Rather, the present results appear to be consistent with the work of Lee et al. [38] who report the appearance of hydroxyl radicals being due to the interaction between anatase TiO_2 and H_2O_2. The divergence in results may be due to the stability of some free radicals on rutile being higher than on anatase (see Ref. [39]) and that the buffer solution used in Fenoglio's work [37] may influence the processes taking place.

From the differences observed with respect to the formation of ROS due to the interaction of H_2O_2 and TiO_2, it is probable that the very low concentration of H_2O_2 in the solutions used in the previous works [15–17] is too low for producing oxidizing species, and hence the catalytic effect, in the dark. Similarly, in the work of Rincon et al. [11] it is difficult to be certain that the toxic effect on bacteria present in the mixture TiO_2/H_2O_2 is due to the formation of free radicals as the concentration of H_2O_2 is also very low.

4. Conclusions

The present work demonstrates that MB is degraded by the chemical interaction of TiO_2 particles with H_2O_2, in ambient lighting and in darkness. Indeed, the results confirm that TiO_2 particles and H_2O_2 can produce ROS (hydroperoxyl and hydroxyl radicals) in darkness. The degradation of MB under these conditions could be regulated depending on the H_2O_2 concentration, as well as the TiO_2 particle concentration and size. The strongest effect was achieved by mixing a high amount of TiO_2 nano-sized particles in concentrated H_2O_2.

Acknowledgments

This study was financially support by a FORNY grant through the Norwegian Research Council (grant number 203372). We are thankful for the contributions of Ivana Fenoglio, Emanuele Carella and their group in Turin at large in the development of the methodology for the EPR experiments. Truls Nordby and Ståle Petter Lyngstadaas are acknowledged for helpful discussions and comments to the manuscript.

References

[1] J.A. Cortes, J.F. Perez-Robles, J. Gonzalez-Hernandez, P. Vorobiev, Y.V. Vorobiev, A.G. Garcia, Physical Status Solidi (6) (2011) 1966–1969.
[2] T.T. Tsai, W.P. Sung, W. Song, Environmental Engineering Science 28 (2011) 635–642.
[3] S. Dutta, S.A. Parsons, C. Bhattacharjee, P. Jarvis, S. Datta, S. Bandyopadhyay, Chemical Engineering Journal 155 (2009) 674–679.
[4] D. Friedmann, C. Mendive, D. Bahnemann, Applied Catalysis B: Environmental 99 (2010) 398–406.
[5] M.A. Henderson, Surface Science Reports 66 (2011) 185–297.
[6] P. Pichat, Applied Catalysis B: Environmental 99 (2010) 428–434.
[7] J. Wang, Y.W. Guo, B. Liu, X.D. Jin, L.J. Liu, R. Xu, Y.M. Kong, B.X. Wang, Ultrasonics Sonochemistry 18 (2011) 177–183.
[8] T.Y. Zhang, T. Oyama, A. Aoshima, H. Hidaka, J.C. Zhao, N. Serpone, Journal of Photochemistry and Photobiology A: Chemistry 140 (2001) 163–172.
[9] T. Hirakawa, Y. Nosaka, Langmuir 18 (2002) 3247–3254.
[10] N. Shimizu, C. Ogino, M.F. Dadjour, T. Murata, Ultrasonics Sonochemistry 14 (2007) 184–190.
[11] A.G. Rincon, C. Pulgarin, Applied Catalysis B: Environmental 63 (2006) 222–231.
[12] C. Randorn, S. Wongnawa, P. Boonsin, Science Asia 30 (2004) 149–156.
[13] S.P. Lyngstadaas, H.J. Haugen, S. Taxt-Lamolle, WO2011080080 (2009).
[14] C. Ogino, M.F. Dadjour, Y. Iida, N. Shimizu, Journal of Hazardous Materials 153 (2008) 551–556.
[15] Y.F. Rao, W. Chu, Environmental Science & Technology 43 (2009) 6183–6189.
[16] X.Z. Li, C.C. Chen, J.C. Zhao, Langmuir 17 (2001) 4118–4122.
[17] B. Jenny, P. Pichat, Langmuir 7 (1991) 947–954.
[18] T. Ohno, K. Sarukawa, K. Tokieda, M. Matsumura, Journal of Catalysis 203 (2001) 82–86.
[19] K. Rezwan, Protein treated aqueous Colloidal Oxide Particle Suspensions: Driving Forces for Protein Adsorption and Conformational Changes, Swiss Federal Institute of Technology (ETH), Zürich, 2005.
[20] R.W. Matthews, Journal of the Chemical Society: Faraday Transactions I 85 (1989) 1291–1302.
[21] B. Liu, L. Wen, K. Nakata, X. Zhao, S. Liu, T. Ochiai, T. Murakami, A. Fujishima, Chemistry 18 (2012) 12705–12711.
[22] K. Murugan, T.N. Rao, A.S. Gandhi, B.S. Murty, Catalysis Communications 11 (2010) 518–521.
[23] G. Marban, T.T. Vu, T. Valdes-Solis, Applied Catalysis A: General 402 (2011) 218–223.
[24] M.R. Hoffmann, S.T. Martin, W.Y. Choi, D.W. Bahnemann, Chemical Reviews 95 (1995) 69–96.
[25] B.J.P.A. Cornish, L.A. Lawton, P.K.J. Robertson, Applied Catalysis B: Environmental 25 (2000) 59–67.
[26] Y.K. Du, J. Rabani, Journal of Physical Chemistry B 110 (2006) 6123–6128.
[27] E.I. Kapinus, T.A. Khalyavka, T.I. Viktorova, Russian Journal of Physical Chemistry 80 (2006) 1240–1243.
[28] N.P. Xu, Z.F. Shi, Y.Q. Fan, J.H. Dong, J. Shi, M.Z.C. Hu, Industrial & Engineering Chemistry Research 38 (1999) 373–379.
[29] L. Pan, J.J. Zou, X.W. Zhang, L. Wang, Journal of the American Chemical Society 133 (2011) 10000–10002.
[30] G.R. Buettner, L.W. Oberley, Biochemical and Biophysical Research Communications 83 (1978) 69–74.
[31] V. Brezova, D. Dvoranova, A. Staško, Research on Chemical Intermediates 33 (2007) 251–268.
[32] J.M.C. Gutteridge, B. Halliwell, Annual New York Academy of Science 899 (2000) 136–147.
[33] C. Frejaville, H. Karoui, B. Tuccio, F. Lemoigne, M. Culcasi, S. Pietri, R. Lauricella, P. Tordo, Journal of the Chemical Society: Chemical Communications (1994) 1793–1794.
[34] T.A. Vestad, ESR Spin Trapping, University of Oslo, 1999.
[35] C.M. Lousada, A.J. Johansson, T. Brinck, M. Jonsson, Journal of Physical Chemistry C 116 (2012) 9533–9543.
[36] A. Lipovsky, L. Levitski, Z. Tzitrinovich, A. Gedanken, R. Lubart, Photochemistry and Photobiology 88 (2012) 14–20.
[37] I. Fenoglio, G. Greco, S. Livraghi, B. Fubini, Chemical European Journal 15 (2009) 4614–4621.
[38] M.C. Lee, F. Yoshino, H. Shoji, S. Takahashi, K. Todoki, S. Shimada, K. Kuse-Barouch, Journal of Dental Research 84 (2005) 178–182.
[39] A.L. Attwood, D.M. Murphy, J.L. Edwards, T.A. Egerton, R.W. Harrison, Research on Chemical Intermediates 29 (2003) 449–465.